ADVANCED FUNCTIONAL MATERIALS
www.afm-journal.de

Optical Switchers to Manipulate Intracellular Pathways and Boost Tissue Regeneration

*Natalia Dell'Aversano, Maria Laura Amenta, Massimo Rippa, Maria Moros, Angela Tino, and Claudia Tortiglione**

The possibility to remotely manipulate intracellular pathways in single cells is among the current goals of regenerative medicine, demanding new strategies to enhance tissue repair and reprogram stem cell activity. Plasmonic nanomaterials are addressing this need, due to improvements in the controlled synthesis allowing convenient regulation and precise thermal positioning. Leveraging on the thermal properties of gold nanoprisms (AuNPs) and on the unparalleled regenerating capabilities of the small invertebrate Hydra vulgaris, here the possibility to activate the molecular machinery underlying the animal regeneration by using AuNPs and applying regular pulses of near infrared irradiation (NIR) is shown. The efficiency of the head regeneration, reproductive capability, and stem cell proliferation rate are boosted by the AuNP photostimulation, indicating NIR triggered hyperthermia as new tool to enhance tissue regeneration. By transcriptional profiling of key developmental genes in animals exposed to external heat or irradiated an estimation of the heat developed in vivo by intracellular nanoheaters is obtained, revealing Hydra as a living thermometer to test performance of plasmonic materials. These results shed light on a novel function of heat emitting nanoparticles to control cell stemness through the activation of molecular pathways that can be targeted for regenerative medicine or wound healing strategies.

1. Introduction

Regeneration, commonly defined as the replacement of body parts lost by injury, can vary greatly among species, tissues and life stages. Basal animals, like cnidarians and planarians, can regenerate their whole body, while most vertebrates and mammals have only limited regeneration capacity, restricted to some tissues (intestinal epithelium, skin, liver, blood, skeletal muscle).[1] In these species tissue repair occurs through inflammation, proliferation, and replacement of the damaged tissue with an acellular fibrotic matrix (scar tissue), which is different from the original tissue. Regenerative medicine strives to identify the mechanisms underlying regeneration of missing structures or repair of damaged tissues with the final aim to control the cells that execute these programs, that is, the endogenous stem cells. In addition, genetic and biochemical factors, acting at cell and tissue levels, and physical stimulations (heat, electric fields, light irradiation) provide pivotal instructive roles for the coordinated behavior of large tissue regions healing the wound.[2] Light exposure (from laser and LED sources) already showed the beneficial effects on wounds, promoting the healing process[3] while thermal therapy has been applied since ancient history, and in daily life people apply a hot compress to reduce inflammation, relieve pain, and improve blood circulation. The heat shock response is one of the best studied exogenous cellular stresses, that has been triggered for therapeutic purposes. A plethora of cellular responses have been characterized, from the induction of the heat shock proteins to alteration of cell-cycle, DNA related processes and apoptotic pathways.[4] The understanding of the influence of heat on the behavior of cells and tissues for promoting the tissue repair and the regeneration is however very complex.[5] The magnitude and the duration of the temperature enhancement dictate the biological outcomes and severe effects, like cell death, can be induced above certain temperatures, which justifies the development of numerous anticancer strategies based on thermoablative techniques.[6] Beside radiofrequency ablation, microwave ablation, and high-intensity focused ultrasounds, widely validated for anticancer clinical practices, nanostructured heat emitting materials are being thoroughly

N. Dell'Aversano, M. L. Amenta[+], M. Rippa, A. Tino, C. Tortiglione
Istituto di Scienze Applicate e Sistemi Intelligenti "E. Caianiello"
Consiglio Nazionale delle Ricerche
Via Campi Flegrei 34, Pozzuoli 80078, Italy
E-mail: claudia.tortiglione@cnr.it

M. Moros
Instituto de Nanociencia y Materiales de Aragón
INMA (CSIC-Universidad de Zaragoza)
C/ Pedro Cerbuna 12, Zaragoza 50009, Spain

The ORCID identification number(s) for the author(s) of this article can be found under https://doi.org/10.1002/adfm.202405400

[+]Present address: Istituto di Bioscienze e Biorisorse, Consiglio Nazionale delle Ricerche, Via Pietro Castellino 111, Napoli 80131, Italy

DOI: 10.1002/adfm.202405400

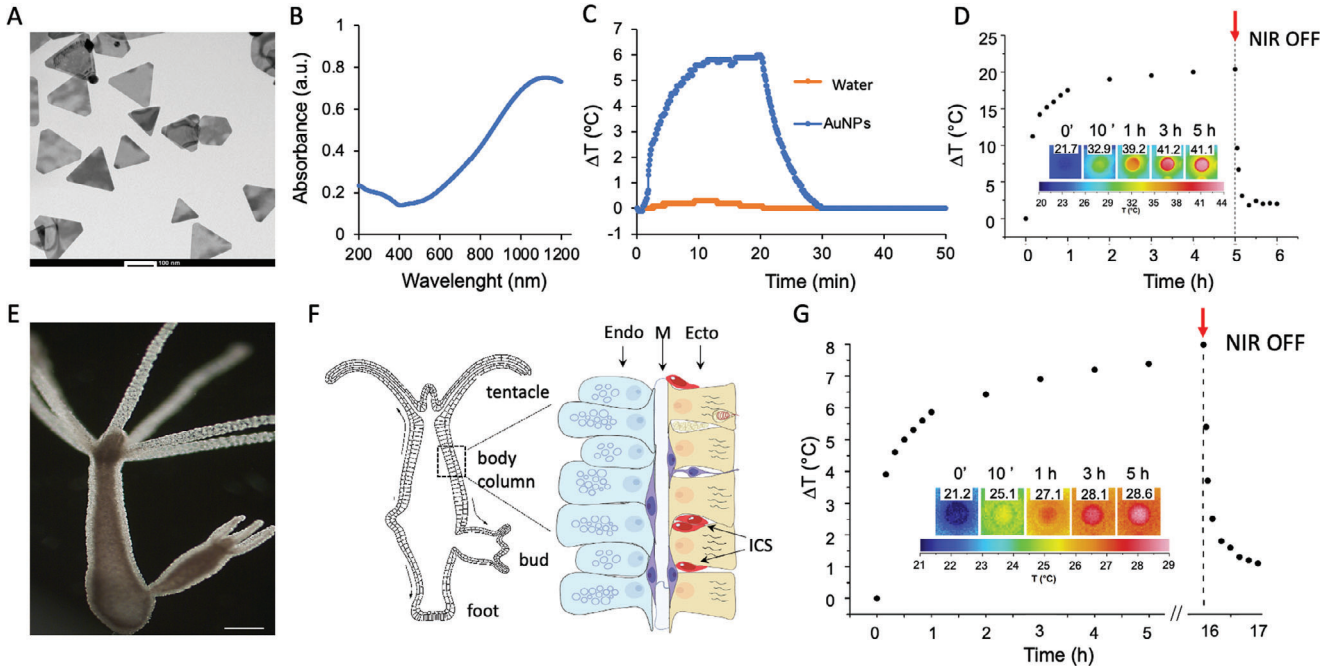

Figure 1. AuNP optical and thermal characterization in vitro and in vivo. A) TEM analysis shows the prism like morphology of the AuNPs and the homogenous preparation. Scale bar = 100 nm. B) UV–vis-near-infrared spectra showing the LSPR peaking at 1080 nm. C) Temperature curves of AuNPs placed in a quartz cuvette and irradiated using a NIR laser at power density 3.9 W cm^{-2}. When a maximum was reached, the laser was turned off and the drop in the temperature was recorded. Pure water (orange curve) was used as control. D) Temporal thermal variation ΔT of AuNP in Hydra medium during and after NIR irradiation (2.42 W cm^{-2}) measured by thermographic technique. The inset shows representative thermal frames acquired during irradiation at the indicated time. The dotted line indicates the laser drop off. E) Image of a *Hydra* showing the simple anatomy with a head surrounded by tentacles. Scale bar 500 µm. F) Scheme of the longitudinal section showing the ectoderm (ecto, light brown) and endoderm (endo, azure) separated by an acellular matrix, the mesoglea (M). The interstitial stem cells (ISC, red) lye into the interstices of the ectoderm giving rise to a few differentiated cell types, including neurons (violet). The arrows indicate the cell migration in the gastric region during the budding process. G) Temporal thermal variation ΔT of living polyps ($n = 15$) treated with AuNP during and after NIR irradiation. The inset shows representative thermal frames acquired during irradiation. The average temperature of each well is reported, while the thermal profile of a single well is shown in Figure S1C (Supporting Information). The temperature is uniform over most of the well area.

investigated to enable controlled delivery of heat inside the cells and avoiding nonspecific damages to adjacent normal tissues.[7] However, their use to augment the tissue regenerative potential has been rarely considered.[8] Indeed, rather than promoting cell death, the local delivery of low heat doses may affect cell fate and decision, cell proliferation rates and modulate specific pathways with beneficial outputs for the cell, as extensively reviewed.[9]

In order to translate these potentials into novel opportunities for regenerative medicine several challenges must be addressed, from the long and expensive in vivo tests on vertebrates, posing ethical issues, to the availability of stable, biocompatible, and heat-emitting materials allowing convenient regulation and precise thermal positioning. Plasmonic materials such as gold nanoparticles have been used as nano-hotspots to selectively generate heat in a spatiotemporal fashion.[8,10] Their eminence is governed by the high biocompatibility and tuneable synthesis, enabling the control of light absorption in the NIR spectral range (690–1100 nm), where tissues are maximally transparent, and the light to heat conversion efficiency.[11] To exploit the possibility that gold nanoparticles act as optothermal actuators to enhance tissue regeneration, the understanding of their in vivo performance to modulate cell functions following stimulation is needed.

Cnidarians and in particular *Hydra vulgaris* have a long history as models for regeneration due to their spectacular ability to rebuild any missing body part from tiny pieces of tissue.[12] The millimeter sized *Hydra* polyp presents a very simple structural anatomy, with a body column and a mouth surrounded by a tentacle crown. The body wall is a bilayer of two cell sheets, an inner endoderm and outer ectoderm that continuously divide, migrate toward the body extremities and together with stem cells interspersed in between the two layers ensure a constant cell turnover and differentiation process, drive asexual reproduction by budding, and maintain constant animal size (**Figure 1**). The softness and transparency of the epithelia enabled to investigate the interaction and the fate of several nanoparticles within the animal tissue by using a variety of optical, ultrastructural and spectroscopic techniques, depending on the chemical composition.[13] Several studies were performed with gold nanoparticles of different shapes and surface functionalization, revealing full biosafety of the material and the possibility to test them in *Hydra* for diverse biological purposes, from drug delivery,[14] to cell thermoablation[15] and in some case the mechanisms underlying their bioactivity were identified.[16] In case of mild hyperthermia mediated of iron oxide nanoparticles an intracellular increase of temperature of ≈10 °C was estimated by comparing the molecular response produced by the magnetothermal

stimulation and by the external heat.[17] Importantly, this study depicted the thermal response of *Hydra* to considerable increase of the temperature (ΔT) above the normal culturing condition (18 °C), demonstrating the absence of morphological damages at 28 °C, the induction of apoptosis and stress responsive gene (*Hsp70*) expression at 30 °C (with negligible morphological effects), and the induction of animal death from 34 °C onward. These results provide the ground for the development of alternative nanoheaters, mediating the delivery of low heat doses, whose potential may be exploited for promote beneficial effects on cell activity rather than inducing programmable cell death.

Here we exploited the possibility to enhance the regenerative potential of *Hydra* by re-activating the stem cell self-renewal through AuNP mediated delivery of heat. By dissecting the response of optothermal stimulation at whole animal, cell, and molecular levels and by comparison to the response induced by external heating, we show the potential of AuNPs to act as novel optical switchers to augment, in situ, the regenerative capability of a whole animal through the manipulation of molecular programs. Drawing inspiration from *Hydra* results the controlled hyperthermia mediated by AuNP represent an innovative tool to promote by the simple use of light regenerative programs following injury and in all pathological contexts demanding to reactivate the stem cell regenerative potential for therapeutic purposes.

2. Results and Discussion

2.1. AuNP Optical and Thermal Characterization In Vitro and In Vivo

AuNP synthesis was performed as previously reported,[16]using sodium thiosulfate to reduce chloroauric acid. Thereafter AuNPs were coated with poly (ethylene glycol) to confer stability. After the purification steps to remove reagents and by-products, the AuNPs were thoroughly characterized for morphology, optical and thermal properties. TEM images (Figure 1A) showed AuNPs of 152 ± 34.9 nm mean length per 10 nm of width, while the UV−vis-near-infrared spectra (Figure 1B) indicated a Localized Surface Plasmon Resonance (LSPR) peaking inside the NIR range (1080 nm), as previously observed.[18] The possibility to convert light into heat was assessed recording the temperature profile of NIR laser-activated AuNP suspensions by using a thermocouple inserted into AuNP solution after NIR irradiation.[19] Figure 1C shows that the temperature of the AuNP solution increases exponentially upon laser illumination, reaching the equilibrium after ≈20 min ($\Delta T = 6$ °C), and then returns to the ambient value after discontinuing irradiation. Pure water at the same laser energy does not induce a significant temperature increase, indicating that the temperature increase with the presence of AuNPs is exclusively attributed to the heat transduced from the light by the AuNPs. A similar trend of the temperature profile was obtained at higher power density (Figure S1A, Supporting Information), reaching a $\Delta T = 37.3$ °C, highlighting the possibility to precisely control the AuNP heat transduction and in turn the biological outcomes, from cell ablation, extensively exploited by us in vitro and in vivo,[15,17,18] to mild effects, object of this study.

As the AuNP thermal properties following internalization may profoundly differ from those measured in monodispersion, the thermal temporal response of the AuNP solution was also determined by thermographic technique, a well-known non-invasive method that allows measurement of spatial temperature distributions and temporal trends accurately.

Figure 1D shows the temporal trends of the average temperatures variance $\Delta T(t)$ measured for the AuNP in Hydra medium (black points), investigated both during and after (NIR OFF) laser irradiation. While the irradiation itself caused a negligible temperature increasing measured on pure medium ($\Delta T = 1.9$ °C), the AuNP solution shows a temporal trend characterized by a rapid initial growth reaching 80% of the ΔT_{max} in ≈40 min. Subsequently, the growth of ΔT is slower, tending toward a plateau reaching after 5 h a maximum temperature variation of $\Delta T_{max} = 20.4$ °C. When the laser is turned off, the sample investigated shows an exponential thermal decrease with a time constant of $\tau = 3.5$ min.

The biosafety of AuNPs following internalization in Hydra polyps was confirmed by treating polyps with increasing concentrations of AuNPs, from 0.5 to 2 mg mL^{-1} and monitored every 24 h, up to 72 h. *Hydra vulgaris* is very sensitive to aquatic pollutants and the response to exogenous contaminants can be assessed by morphometric assay, detecting body and tentacle damages, followed by behavioral and molecular assays.[20] In Figure 1E a healthy polyp is shown, together with the anatomical structure, showing the body wall composed by epitheliomuscular cells lining the inner side (endoderm) and the outer side (ectoderm) and the interstitial stem cells (ISC) differentiating in a few cell types (neurons, gland cells, and nematocytes). No morphological damages were detected in presence of AuNPs (Figure S2A, Supporting Information), confirming previous evidence on full biosafety of AuNP in *Hydra* tissue.[15,16] Using Inductively Coupled Plasma Optical Emission Spectroscopy (ICP-OES), the efficient internalization of AuNPs into *Hydra* was estimated (103 ± 2.4 ng Au/polyp), confirming data by optical microscopy using fluorescent labeled AuNP,[16] previously reported (Figure S2B, Supporting Information).

The thermographic technique was next employed to determinate in vivo the thermal profile of AuNP treated animals irradiated for increasing periods of time (Figure 1G). The irradiation itself caused a negligible temperature increase measured on the well hosting living animals untreated that reaches after 5 h a variance $\Delta T = 1.6$ °C (Figure S1B, Supporting Information). In the case of AuNP treatment a trend similar to that reported in Figure 1D was obtained but with different characteristic thermal values. The presence of AuNPs caused a rapid increase of the temperature over the first hour of irradiation, continuing at a lower rate over the following hours and reaching a maximum value $\Delta T_{max} = 7.4$ °C after 5 h. Prolonging the irradiation time up to 16 h does not cause a further increase of the temperature. When the laser is turned off, also in this case the thermal recovery shows a decreasing exponential trend characterized by a higher time constant ($\tau = 6.2$ min) than the case of Figure 1D. Notably, a similar thermal trend was measured from a single animal under the same condition ($\Delta T = 5.9$ °C), showing a negligible contribute of heat dissipation and transfer among the animals on the detected temperature (Figure S1D, Supporting Information) and suggesting a highly localized light to heat conversion into the animal tissues.

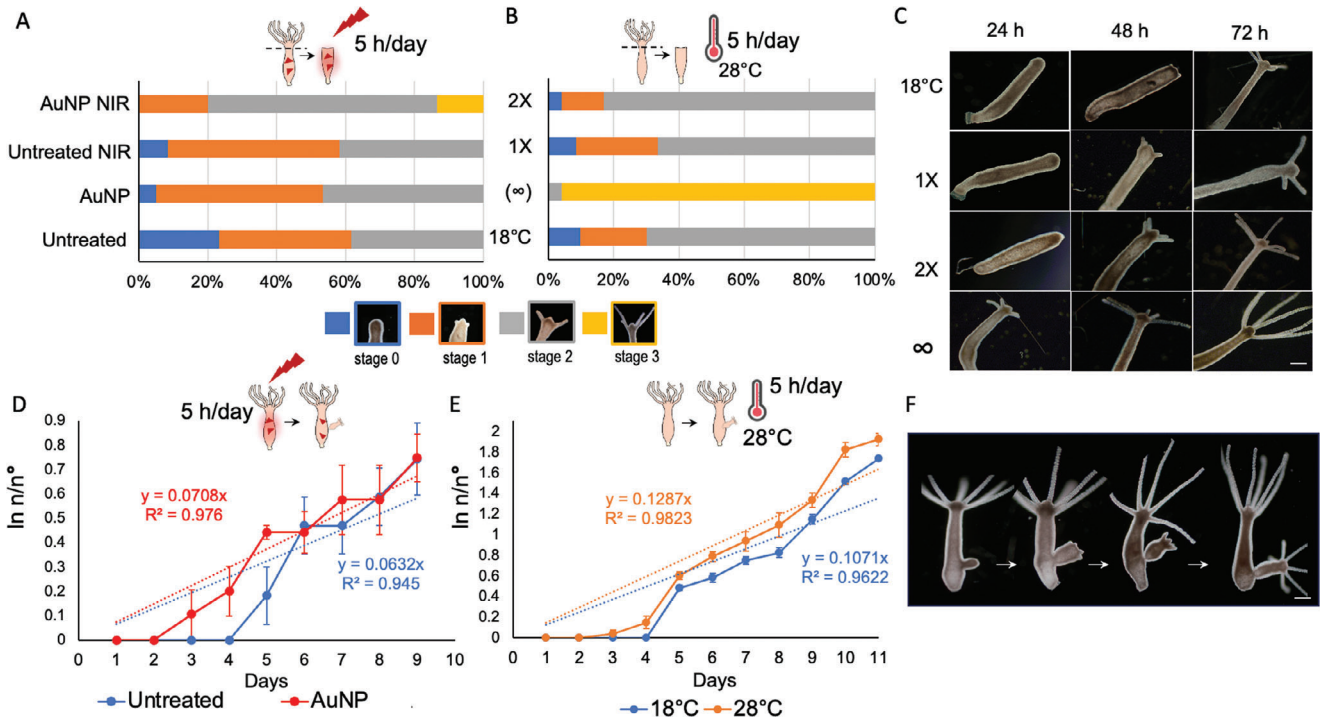

Figure 2. Opto-thermal stimulation of AuNP enhance regenerative and reproductive capabilities of living Hydra. Whole polyps treated with AuNPs were bisected and allowed to regenerate the head under NIR light (condition AuNP NIR) or ambient light (AuNP). As control conditions untreated and untreated illuminated animals were used. The percentage of regenerating heads were scored every 24 h based on their developmental stage: stage 0 (blue), stage 1 (orange), stage 2 (gray) and stage 3 (yellow). Figure S3 (Supporting Information) reports the stage distributions at 24 and 72 h p.a. B) Whole polyps were bisected and exposed to external heat either continuously (infinite symbol) or for 5 h /day. 1X = one pulse of heat (28 °C), 24 h p.a.; 2X = two pulses of heat, 48 h p.a. For each condition three independent biological replicates were performed ($n = 60$). Statistical comparisons are reported in Tables S1 and S2 (Supporting Information). C) Representative microscopic images showing morphology of regenerant polyps in each condition. Scale bars 500 µm. D) The graph shows the growth rate of a population from 3 founder animals either AuNP treated (red curve) or untreated (blue curve) and NIR illuminated for 5 h/day. The logarithmic growth rate constant (k) is the slope of the regression line. E) Growth rate of a Hydra population exposed to 28 °C for 5 h/day (orange curve) and compared to animals grown at 18 °C (blue curve). F) Representative microscopic images showing the budding process. Scale bar, 500 µm.

2.2. AuNP Photostimulation Enhances *Hydra* Head Regeneration and Reproduction Efficiencies

The regeneration of a new head post amputation (p.a.) has been extensively characterized in *Hydra* both at morphological and molecular levels.[12c] Within the first hour p.a. the site of injury responds by re-organization of the epithelial cells to close the wound, the body stump appears as a headless moiety without gross morphological changes (stage zero) up to 30–36 h, when small tentacle buds begin to emerge on the regenerating tip beginning the process of morphological differentiation of cells (stage 1). Over the next 24 h the emerged tentacles progressively growth in length (stage 2) completing the process by 72 h, when the whole tentacles are enough to catch the prey (stage 3) (**Figure** 2A). Despite the studies on the effects of the temperature on *Hydra* viability, showing thermotolerance, acclimatation, and capability to adapt to elevated environmental temperatures,[21] a detailed characterization of the effect of temperature on the dynamic of the regeneration is lacking, except rare report from the past century.[22] Recent studies by functional calcium imaging showed that extended exposure to elevated temperatures did not affect various behavioral features in *Hydra*,[23] while short thermal stimulation drives temperature-dependent firing rate in specific Hydra neurons.[24] However, these studies focus on neural responses and not on regenerative capabilities. Thus, we exploited the possibility that the temperature increase induced by the AuNP photo-thermal stimulation might positively affect the dynamic of this process by irradiating amputated bodies for 5 h each day, that is, the period of time sufficient for AuNP to reach the ΔT_{max}.

The biodistribution of the developmental stages at 48 p.a. (the optimal temporal window for quantify morphological differences) showed a significant increase in the percentage of stage 2 and stage 3 as effect of the AuNP photostimulation compared to the other conditions, suggesting an acceleration of the dynamic of the regeneration (Figure 2A). A similar effect was observed by exposing amputated polyps, in absence of AuNPs, to an external heat source (incubator warmed at 28 °C) either continuously or as pulses of 5 h per day (Figure 2B,C). While after a single pulse (1X) the percentage of animals at the different stages were similar to controls, after 2 pulses (2X) the percentage of stage 2 was significantly higher, revealing the dependency of the regeneration on the number of heat pulses and on the duration of the thermal stimulus. Interestingly in case of continuous incubation at 28 °C, all animals reached stage 3, that is, full head regeneration, indicating a 24 h anticipation of the whole process. Figure S3

(Supporting Information) shows the distribution of the regenerative stages obtained by photostimulation and external heating also at 24 and 72 h p.a., confirming the acceleration of the process induced by the moderate heat.

Beside regeneration, the reproductive capability of the polyps was also monitored. The tissues of *Hydra vulgaris* are extremely plastic and dynamic, and the balance between cell production and loss underlies a constant body size.[25] Epithelial cells continuously divide migrate toward the animal ends contributing to the formation of new individuals, budding from the gastric region, and detaching from the mother in ≈3 days[26] (Figure 2F). Under controlled environmental conditions, the speed of growth depends solely on the speed of epithelial cell division, however, numerous environmental factors can influence this process.[26] To evaluate the impact of AuNP on the population growth rate, groups of three founding mothers were treated with AuNP, daily fed, and exposed on alternate days to pulse of 5 h of NIR illumination. The graph of Figure 2D shows since the beginning of the monitoring clear differences in the number of individuals generated by AuNP treated mothers compared to untreated. The slopes of the linear regression lines, representing the growth rate (k) of the two populations, are different among the two conditions, being higher for treated animals (0.071) compared to the untreated (0.063), confirming the effect mediated by AuNP photostimulation on the population growth. A similar enhancement of growth rate was obtained by exposing the polyps to 28 °C (Figure 2E), showing a general effect of the temperature increase, produced by intracellular nanoheaters or by an external macroscopic source on *Hydra* budding.

2.3. Molecular Pathways Activated by Optical Switchers

Both processes of regeneration and budding rely on stemness of interstitial and epitheliomuscular cells continuously undergoing self-renewal by mitotic division and differentiation.[27] Unbalancing of these processes may affect the dynamic and the efficiency of both phenomena. To estimate whether the enhanced regeneration and reproduction in photostimulated polyps positively correlates with the cell proliferation rate, a quantitative estimation of the dividing cells was performed, by mean of Bromodeoxyuridine (BrdU) assay. This assay is based on the capability of this Thymidine analog to be incorporated into DNA in place of Thymidine and to be detectable by an immunoassay, allowing to quantify the cells that are undergoing or have recently undergone DNA replication. Treated animals were dissociated into a suspension of fixed single cells maintaining their morphology (a process named maceration)[28] and the $BrdU^+$ cell relative abundance (labeling index) was monitored at 5 h and 16 h p.a. (**Figure 3A**).

At both time points the percentage of fast cycling interstitial stem cells (ISC), normally completing a cell cycle in 18–30 h,[29] were found significantly increased in AuNP treated and irradiated animals compared to other conditions (Figure 3B–D), and this trend was observed also for the epithelial cell (EPI) proliferation rate, although at a minor extent (Figure 3C–E), which agrees with their slower cell cycling activity (48–72 h).[30] Of note, the NIR irradiation caused per *sè* a significant inhibition of both EPI and ISC cell proliferation, revealing the capability of AuNP photostimulation not only to fully prevent this effect but to further boost the proliferative activity. Regenerants exposed to a macroscopic heat source (28 °C) also showed at both time points increased cell proliferation rates, but limited to the EPI (Figure 3G–I) and not ISC (Figure 3F–H), which well explain the in vivo enhancement of the reproduction capability, driven by EPI cells. Despite great knowledge on the *Hydra* ISC role in maintaining tissue homeostasis,[27a,b] the molecular mechanisms underlying stemness are not fully understood to date and are being revisited following recent genomic and transcriptomic data.[27c] Several evidence show they are likely regulated by temperature, metabolic control mechanisms, and growth factor pathways including Wnt and TGF-β signaling.[31] In line with these evidence, we searched for the involvement of known molecular regulators of self-renewal and differentiation of *Hydra* stem cells by transcriptional profiling of key genes, such as the transcription factors *forkhead box O (FoxO)*, and two genes belonging to the Wnt/β-catenin signalling pathway, that is, *β−catenin (β-cat)*, and the proto-oncogene *Myc 1*. *FoxO* is one of the critical drivers of stem cell continuous self-renewal. It is expressed in the three cell lineages and its overexpression increased ISC proliferation.[32]Remarkably, it is also responsive to high level of Reactive Oxygen Species (ROS), representing a marker for the oxidative and heat stress.[33] *β-cat* also acts as a positive regulator of stem cell proliferation,[34] as shown by the increased stem cell density in transgenic animals overexpressing β-catenin. It plays also other regulatory function in the stem cell balance, controlling downstream target genes, including the negative regulator of the stem cell self-renewal, *Myc1*.[35] The Superoxide Dismutase gene (*SOD*) was also considered in our analysis, previously shown overexpressed in the antioxidative processes triggered by stressor exposure,[36] including heat, and in response to short pulses of NIR irradiation.[16] The modulation of gene expression in polyps treated by AuNP and NIR irradiated for 5 h was tested by quantitative real time reverse transcription PCR (qRT-PCR), a technique allowing to measure the mRNA levels of a specific gene, relative to an internal control.[37] The heat map of Figure 3J used to illustrate differential gene expression data by color coding the magnitude of values, shows a significant decrease of *β-cat* and *Myc1* transcript levels in AuNP treated and illuminated polyps, compared to other conditions, suggesting an active role of these transcription factors controlling the ISC self-renewal. Their transcriptional regulation may account for the increase in the ISC density observed at cell level. In line with this finding, the positive regulator *FoxO* was found strongly upregulated in AuNP and NIR illuminated polyps, and in agreement with its role to drive ISC self-renewal this may explain the ISC boost induced by the photostimulation. The additional *FoxO* responsiveness to cellular stressors, including heat, clearly indicates the effective light-heat conversion occurring in AuNP NIR polyps, and not in other conditions, suggesting the thermal stimulus as main trigger of the enhanced regeneration. The upregulation of a second stress responsive gene, *SOD*, specifically in AuNP NIR polyps, further supports the increase of temperature induced by intracellular nanoheaters as main signal triggering the modulation of gene expression. These data were paralleled in the animals exposed to external heat, allowing to estimate the ΔT changes produced in vivo by AuNPs.

Inspired by the transcriptional data underlying the cell turnover and collected at the single time point of 5 h p.a., we

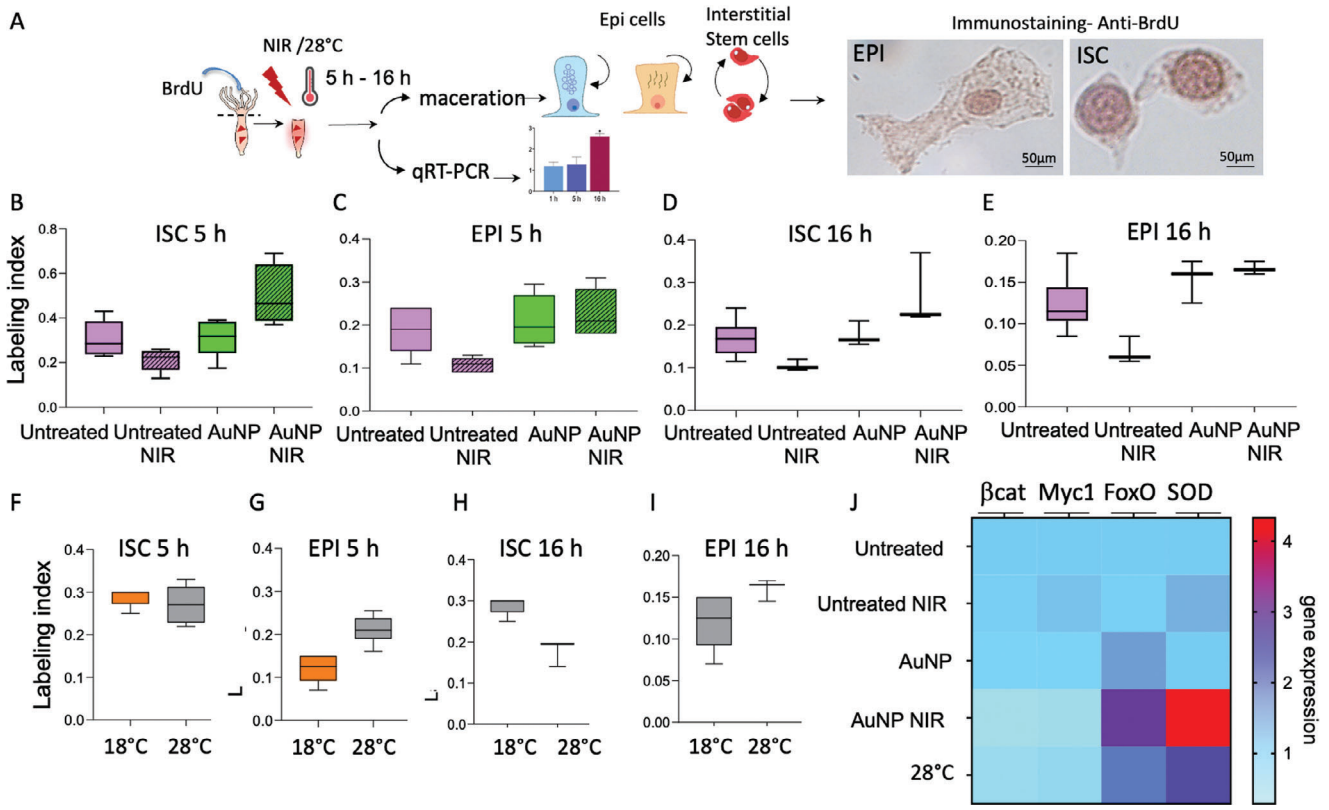

Figure 3. Photostimulation of AuNP augments stem cell proliferation rates during regeneration. A) Scheme of the experimental procedure. *Hydra* polyps were treated with AuNPs and BrdU, amputated, and allowed to regenerate missing heads before maceration and immunostaining, or processing for qRT-PCR. Representative images of $BrdU^+$ EPI and ISC cells are shown on the right. B–E) Impact of AuNPs on cell proliferation rate, measured at 5 h p.a. and 16 h p.a. as percentage of $BrdU^+$ nuclei of B–D) ISC cells and C–E) EPI cells in each experimental condition. Statistical analysis is provided in Tables S3 and S4 (Supporting Information). F–I) Effect of thermal stress ($\Delta T = 10°$) on cell proliferation of F–H) ISC cells and G–I) EPI cells macerated from untreated animals. For each graph data are presented as means and min to max values of three biological replicates ($n = 3 \times 200$ cells). Statistical analysis is provided in Tables S5 (Supporting Information). J) Heat map summarizing expression data for 4 genes exhibiting differential expression across five conditions, analyzed 5 h p.a. The gene names are shown on the top. Each column of the heat map represents a gene, each row represents a condition, and each cell displays gene expression values, ranked by mean expression value versus mean expression value of untreated condition along the vertical axis. Three biological replicates, each with three technical repeats were performed. The corresponding histograms and statistical analysis are shown in Figure S4 (Supporting Information).

suspected that the acceleration of the regenerative process might be caused by an earlier activation of developmental genes, and that AuNPs may function as optical switchers of molecular pathways. To this aim, we characterized the dynamic of the expression of two well-known developmental genes belonging to the *Wnt/β–catenin* signaling pathway, *T-cell factor* (*TCF*) and *Sp5*, both highly expressed in the early phase of head regeneration (from 3 h p.a. onward).[38]

Their differential expression was assessed on a time course, with three-time points p.a. (1, 5, and 16 h) in response to either AuNP photostimulation or to the external heat (18, 24, and 28 °C). The lower part of the heat map (**Figure** 4C,E) and Figure S5 (Supporting Information) show for both genes the increased transcription at 16 h p.a., confirming temporal expression data already published,[13b,38b,39] independently from the environmental temperature. By contrast, a clear upregulation of *TCF* expression was observed in irradiated polyps, but not in other conditions, already at 1 h p.a., indicating an anticipation of the molecular events normally occurring at 16 h p.a. (Figure 4A,B). This upregulation was less pronounced at 5 h p.a., and absent at 16 h p.a., possibly due to the already high levels of transcripts at this time p.a. In case of *Sp5*, a similar anticipation of the transcription was observed at 5 h p.a. in AuNP irradiated animals and not in other conditions (Figure 4A–D). The faster dynamic of activation of these two important genes might explain at molecular level the faster regeneration observed at morphological level, and suggest additional upstream players transducing the thermal stress signal into transcriptional activation of developmental genes. Increased ROS levels have also been suggested in the enhanced regeneration induced by photostimulation of organic semiconductor nanoparticles in Hydra.[40] Together with increased Ca^{2+} levels, stress induced MAPK signaling through *c*-Jun N-terminal kinases (JNKs), and extracellular signal-regulated kinases (ERKs) they all represent possible players,[41] to be further investigated in the future. A model summarizing the biological pathways induced by the AuNP photostimulation is shown in **Figure 5**.

Gold anisotropic nanoparticles present unique plasmonic properties that can be exploited for therapeutical purposes. Their potential of "light to heat" conversion has been widely proposed for anticancer strategies based on cell thermo ablation,[42] while

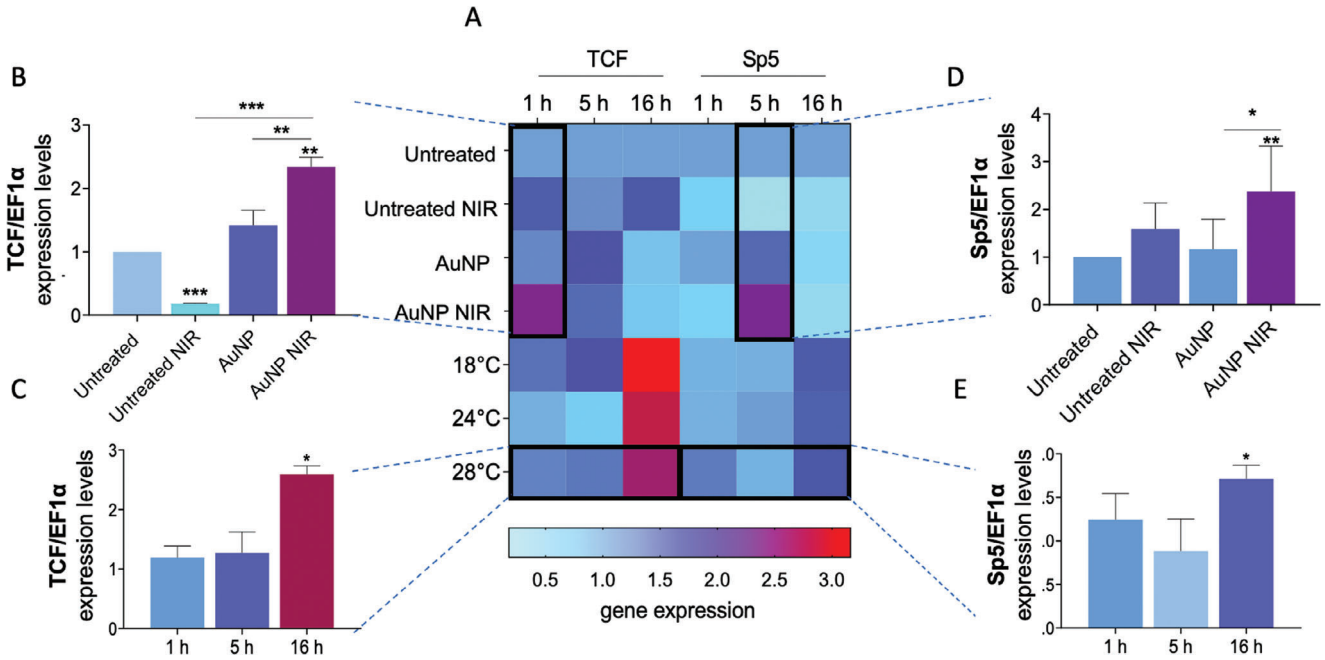

Figure 4. AuNP act as optical switchers of molecular pathways boosting stem cell proliferation. For the time-course gene expression profiling of *Hydra* response to NIR stimulation amputated polyps (either untreated or AuNP treated) were exposed to NIR light (or ambient light) and allowed to regenerate missing heads for the indicated time p.a., before RNA extraction and quantification of *TCF* and *Sp5* transcripts by qRT-PCR. A) The heat map summarizes the expression data for *TCF* and *Sp5*, exhibiting differential expression across diverse conditions and analyzed at 1, 5, and 16 h p.a. Each cell displays gene expression values, ranked by mean expression value versus mean expression value of control (untreated) along the vertical axis. B) The *TCF* mean expression levels within the black frame (column 1 h) are reported as histogram, to highlight statistically significant differences among the conditions. The same graphic representation of the *TCF* mean expression levels (black framed, from the row 28 °C) are shown in C. D) *Sp5* mean expression levels within the black frame (column 5 h) expanded in the relative histogram. E) *Sp5* temporal expression pattern at 28 °C represented as histogram. Data are the average of three independent biological replicates, each performed with 15 animals, and three technical repeats. Statistical analysis was performed as either unpaired t-test (to compare samples treated and/or illuminated with each other), or one sample T-test (to compare samples treated and/or illuminated toward the control untreated). $*P < 0.05$; $**P < 0.01$; $***P < 0.001$.

the possibility to use them to drive other processes controlled by mild heat it is in its infancy. In some studies gold nanoparticles embedded into polymeric or cell scaffolds were found able to promote bone regeneration or to enhance the cell migratory behavior, in vitro.[43] More recently, bacterial produced gold nanoparticles were shown able to in situ amplify the antitumor immune response through NIR triggered mild hyperthermia,[44] reinforcing the transformative concept here presented on their potential to manipulate intracellular pathways rather than promoting thermo-ablative processes.

The main advantage of gold nanoprisms is offered by their tuneable optothermal properties, that can be precisely controlled through the synthesis. NIR light stimulation enables spatial control of heat delivery and thus the possibility to precisely control the outcomes, up to the single cell level. The main drawback hampering wide clinical translation of these photothermal agents is however represented by the profoundly diverse outcome when moving from in vitro to in vivo environment, where the properties of the receiving tissue (thickness, stiffness, transparency) and the complexity of the intracellular environment (salts, proteins, reactive metabolites) affects the physico chemical properties including the thermal behavior. The internalization route (directly through the membrane, by endocytosis or macropynocytosis) may also result in the aggregation into micrometre sized structures, affecting the thermal behaviour characterized in solution. These issues made the measurement of the temperature developed by nanoheaters inside the cells challenging thus far. Sophisticated methods based on thermosensitive molecules were able to determine the absolute temperature at distances below 0.5 nm from the surface of the magnetic nanoparticles,[45] or in the surrounding medium using thermosensitive probes,[46] while for gold nanoparticles tethered lipid membranes were developed to detect the localized heat transfer arising from NIR laser excitation.[47]

A study combining simulation and in vitro experimental data established a correlation between the heat developed by gold nanostars, the tip sharpness and the photothermal cell ablation induced by gold nanostars.[48] Similar theoretical methods dealing with nanoparticles not causing cell death may provide interesting clues to estimate the efficiency of heat developed within biological tissues, together with more versatile methods and suitable in vivo models.

Leveraging on the unique morphological and physiological traits of the small animal model *Hydra* we were able to estimate the heat delivered in vivo following photostimulation of AuNP, by merging data from direct thermographic measurements acquired during AuNP stimulation to the effects induced at whole animal, cellular and molecular levels by a similar heat dose, delivered externally. The estimated increase of temperature $\Delta T =$ 7.4 °C mediated by the AuNP NIR stimulation could reasonably

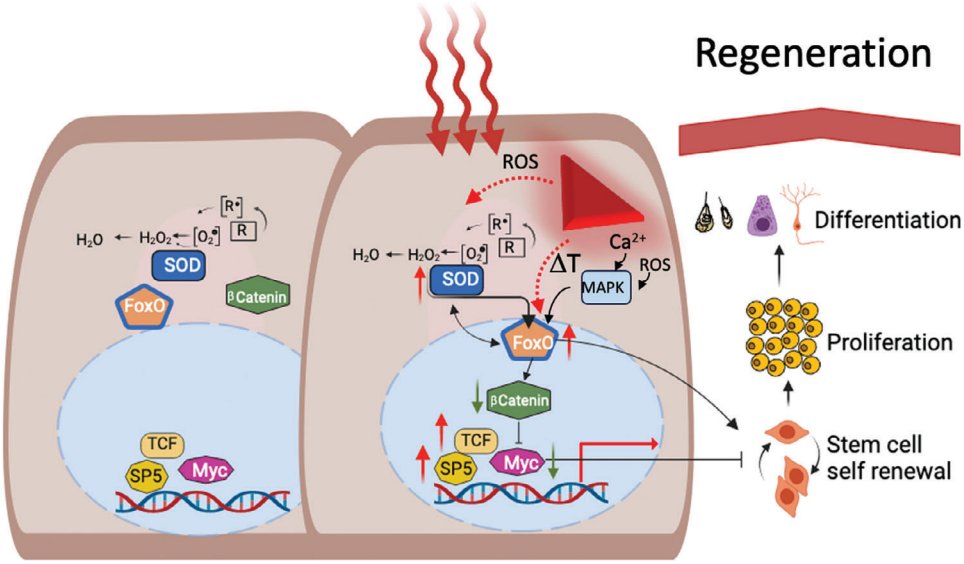

Figure 5. AuNP photostimulation activates molecular pathways underlying stem cell self renewal and promoting regeneration. Schematic of the known molecular regulators of *Hydra* stemness and stress response in homeostatic condition or after injury. Bisecting the animal triggers a cascade of wounding signals, including Ca^{2+}, ROS, and MAPK signaling, finally activating the *Wnt/β−catenin* signalling pathway at the wound site.[27b,41] On the left a stem cell in depicted, showing physiological redox reactions, basal activity of the selected regulators controlling the balance between self-renewal and differentiation maintaining tissue homeostasis. On the right, a model of the biological pathways possibly induced by AuNP optothermal stimulation (wavy lines) in a stem cell: after injury, the heat locally delivered by AuNP irradiation may unbalance the redox state inducing free radical formation (shown as black dot) on different biomolecules present in their neutral form (bracket) in the cell cytoplasm, leading to transcriptional activation of antioxidant genes (*SOD* and *FoxO)*. In addition, the heat stimulus may directly activate *FoxO* and through increased Ca^{2+}, ROS levels, and *MAPK* signaling,[41] modulating the expression of transcriptional factors (*β−cat*, *TCF*, *Sp5*, *Myc1)*. The overexpression of the positive regulators and the downregulation of the *Myc 1* may anticipate the injury related boost of the stem cell activity, promoting self-renewal, proliferation and differentiation of head tissue, leading to full regeneration. Plain black arrows indicate functional data previously published; dashed arrows possible mechanisms; red arrows indicate upregulation and green arrows downregulation from this study. Created with BioRender.com.

explain the outcomes of the multilevel analysis performed in vivo (regeneration and reproductive capabilities), ex vivo (cell proliferation) and in vitro (gene expression), that were found mirroring the effects induced by a similar external heat increase (selected as $\Delta T = 10$ °C to take into account the air-water-animal heat dissipation and the higher local temperatures obtained on the animal in close proximity of AuNPs): the regeneration efficiency was boosted by 5 h long pulses, the reproductive rate was similarly enhanced, the stem cell self-renewal activity was significantly increased by both stimulations, and importantly the modulation of gene expression followed similar transcriptional trends for all selected genes. The expression levels of key developmental genes were found modulated specifically in presence of AuNP and NIR irradiation (upregulation of *FoxO, TCF, Sp5,* and downregulation of *β* catenin and the negative regulator *Myc1*) (Figure 3J), in agreement with functional studies showing their role to promote stem cell proliferation.[27b,32,35b,38a] Despite their independence from the environmental temperature (Figure S5, Supporting Information) their activation in photostimuated animals was found strongly anticipated, laying the bases for the accelerated regeneration observed in vivo.

Although not considering the body-water-air heat dissipation variables and other light-heat energy conversion values, our estimation of the temperature increments developed by AuNP inside the illuminated tissues suggests high stability into the cells and confirms an optimal use in therapeutics. Most importantly it reveals *Hydra* as a living thermometer to test heating performance of plasmonic materials.

3. Conclusion

Despite the growing portfolio of biomedical applications mediated by gold nanoparticles, mainly based on thermo ablation, their potential to control biological function through the delivery of low heat dose has been rarely explored. Here we demonstrate the possibility to use plasmonic nanoparticles to control a fundamental biological process, the tissue regeneration, by the simple use of light. Studying the cellular and molecular mechanisms by which animals regenerate missing parts of the body is of primary interest to improve our comprehension of tissue/organ regeneration in humans and might help to identify novel strategies to rescue the lost regenerative capacity. Our results shed light on a novel function of heat emitting nanoparticles to control cell stemness through the activation of molecular pathways that could be targeted for regenerative medicine or wound healing strategies.

4. Experimental Section

Synthesis of AuNPs: AuNPs were synthesized as reported before.[49] 220 mL of 0.5 mM $Na_2S_2O_3$ was mixed with 60 µL of a solution containing KI 0.1 M. Thereafter, 110 mL of this solution was added dropwise to 200 mL of 2 mM $HAuCl_4$ and left for 4 min. This procedure was repeated

again, 70 mL of $Na_2S_2O_3$ was added and the solution was left for 1 h at room temperature. To stabilize the surface of the AuNPs against precipitation in Hydra medium, SH-PEG-COOH (5 kDa, Rapp Polymere) was added in a 1:2 ratio (AuNPs:PEG, w/w). PEG was diluted in 1 mL of water, $NaBH_4$ was added (1:1 molar ratio of PEG:$NaBH_4$) and the solution was adjusted to pH 12 and sonicated for 1 h (60 °C). PEG excess was removed by centrifugation at 4400 g for 15 min, twice.

AuNP Characterization: **Temperature variation** upon NIR irradiation was evaluated using a 1 mL of the AuNPs (0.5 mg mL^{-1}) in a quartz cuvette (1 cm optical path) with magnetic stirring to prevent AuNP precipitation and to homogenize the temperature in the solution. The AuNPs were irradiated at 3.9 W m^{-2} or 26 W cm^{-2} for 20 min and then the laser was turned off. The temperature was monitored in real time by a thermocouple T-type coupled to a Datalogger USB (TC Direct). The laser source was a solid state continuous-wave (CW) IR laser (Ventus, by Laser Quantum), emitting at 1064 nm and with a beam diameter of 2.2 mm. The exit power was measured by a Power Meter (by Thorlabs).

UV-VIS spectra were collected using a Cary 50 Probe spectrophotometer (Varian Medical Systems (CA, USA).

Transmission electron microscopy (TEM) images were obtained using a FEI Tecnai T20 microscope operating at 200 kV (Laboratorio de Microscopías Avanzadas, Zaragoza, Spain). A single drop of the AuNPs was placed onto a copper grid coated with a carbon film and dried in air. The mean sizes of AuNPs were obtained by averaging >100 particles from the TEM images using ImageJ software.

Elemental analysis by Inductively Coupled Plasma Optical Emission Spectroscopy (ICP-OES). 10 polyps were treated with 1 mg mL^{-1} of AuNPs in a final volume of 300 µL, while untreated polyps were maintained in 300 µL of Hydra medium. Samples were digested with 1 mL of HNO_3 (1 h at 90 °C) and further diluted to 20 mL using milliQ water. Samples were measured in duplicate and evaluated by ICP OES using an Optima 8300 (Perkin Elmer).

Thermographic Measurements: Groups of 15 polyps were treated 24 h with AuNPs (1 mg mL^{-1}), washed three times, and irradiated with a CW NIR laser beam at 2.42 W cm^{-2}, λ = 1064 nm (Thorlabs, M9-A64-0200). Thermographic measurements were carried out using an LWIR AVIO TVS500 camera (Nippon Avionics Co., Yokohama, Japan) with an uncooled microbolometric detector (spectral range 8–14 µm, FPA 320 × 240 pixels and NETD ~60 mK at 25 °C) mounting a 22 mm focal lens with an IFOV 1.68 mrad. The commercial software IRT Analyzer ver. 4.8 (GRAYESS Inc., Bradenton, FL, USA), with which the camera was supplied, was used to manage the camera parameters and for image acquisition. Thermal frames of the well containing living polyp in each experimental condition were recorded before (t = 0 s) and during laser irradiation at different time intervals. For each time of acquisition, ten thermal images were recorded with a frame rate of 5 Hz and the average temperature of the central area (≈20 mm^2) of the well extrapolated. Finally, the temporal trends of the average temperatures variance ΔT was calculated with the following relation $\Delta T(t) = T(t)\text{-}T(0)$. In the analysis an emissivity of 0.96 was considered for the sample investigated. The thermal trend of the samples, measured after laser irradiation, was fitted with the following decreasing exponential function $y(t) = A+B\ exp(-t/\tau)$ and the time constant τ estimated.

Animal Culture: *Hydra vulgaris* polyps were asexually cultured in Hydra medium (1 mM $CaCl_2$ and 0.1 mM $NaHCO_3$) in double-distilled H_2O at pH 7.[50] The animals were kept at 18 ± 1 °C and fed on alternate days with freshly hatched *Artemia salina* nauplii. For all experiments, homogeneous population samples of *Hydra* were selected from adult polyps without buds, 24 h after their last feeding.

Toxicological Assay: Groups of 15 animals were incubated with different concentration of AuNPs (0.5 mg mL^{-1}; 1 mg mL^{-1}; 2 mg mL^{-1}) and placed in a 48-multiwell plate in a final volume of 300 µL of Hydra medium for 72 h. Polyps morphology and tissue integrity was carried out every 24 h using a a stereo microscope (Olympus SZX7). All images were acquired using CellF software (Olympus). Adverse effects, if present, were ranked, assigning a numerical score to progressive morphological alterations, as previously reported.[51]

Hydra NIR Irradiation: For all assays (regeneration, reproduction, cell proliferation, and gene expression) the NIR irradiation was performed by illuminating living polyps placed into a 96-multiwell plate with a CW laser beam (λ = 1064 nm) at power density 2.42 W cm^{-2} (Thorlabs, M9-A64-0200) for the selected time.

Hydra Regeneration Assay: Groups of 20 polyps were incubated 24 h with AuNPs (1 mg mL^{-1}) in final volume of 300 µL. After 3x washes with fresh Hydra medium polyps were bisected (80% of body column length) and exposed to NIR light for pulses of 5 h per day. As control condition untreated irradiated polyps or treated not irradiated polyps were used and the regeneration efficiencies compared in each experiment among the four conditions. Regenerative stages were clustered as stage 0 at wound closure; stage 1 at beginning of tentacle morphogenesis (tentacles appear as buds); stage 2 (tentacles reaching 2/3 of a mature tentacle length) and stage 3 when the process was completed. For stage recording an inverted microscope (Axiovert 100, Zeiss) with a digital color camera (Olympus DP70) was used. The same assay was employed to evaluate the effect of the external temperature. After amputation the polyps were allowed to regenerate in an incubator pre warmed at 28 °C for the duration of the heat pulse and put back at 18 °C for the remaining time.

Hydra Growth Rate: Animals either treated with AuNP or untreated were exposed 5 h/day to NIR light and fed daily for 14 days. The population growth rate of *Hydra* follows an exponential trend and is defined by the constant K, which represents the slope of the linear regression curve obtained from the standard equation: K = ln (n/n°)/t, where t = represents the time (in days), n° = the initial number of individuals, n = the number of individuals at time t.[26,52] Three independent experiments were performed. The same assay was performed on animals exposed for 5 h/day to 28 °C.

Hydra Cell Proliferation Assays: Groups of 10 *Hydra* either untreated or exposed to AuNP 1 mg mL^{-1} were treated for 24 h with 5Bromo-2′-Deoxyuridine BioUltra (Sigma–Aldrich) 5 mM in Hydra solution. After amputation polyps were NIR irradiated for 5 or 16 h, before maceration into single cell suspension. As a control conditions, both untreated and treated animals not illuminated were used. Single cell suspensions were obtained from polyps in each experimental condition by soaking into a maceration solution (acetic acid, glycerol and H_2O in a 1:1:13 v/v ratio) at +4 °C overnight, as reported.[28] Single cells were fixed with paraformaldehyde 4% and spread on slides that were washed with phosphate-buffered saline PBST (PBS 1X-Tween 0,1%) for 1 h at room temperature, treated with 2 M HCl for 45 min at room temperature for acid hydrolysis and washed in PBS for 20 min. Blocking was performed through the addition of BSA-T 1% for 15 min in a wet chamber. Incubations with 1:500 mouse anti-BrdU (Sigma) in BSA-T 1% were done for 2 h in a wet chamber. The preparation was then washed in PBS-T at room temperature and treated with post primary block solution (Novocastra Laboratories ltd) for 30 min. Excess antibody was removed by two 5 min washings with PBS-T at room temperature. Then Novolinker Polymer solution (Novocastra Laboratories ltd) was added for 30 min. The preparations were washed in PBS-T and then incubated in DAB (colorimetric reagent and peroxidase substrate) for 5 min. The reaction between the peroxidase linking to the post primary and DAB was blocked by rinsing the slides in water for 5 min. Slides were mounted using Vectashield Antifade Mounting Media with DAPI (Vector Laboratories) and stored at 4 °C. Slides were observed using an inverted microscope (Axiovert 100, Zeiss) equipped with a color digital camera (Olympus DP70). Images were acquired by the CellF (Olympus) software. $BrdU^+$ cells were detected by their brownish color using a 32x objective and quantified as ratio on a total of ≃600 epithelial cells/slide.

Gene Expression Analysis: Differences in gene expression profiles induced by AuNPs and/or light were assessed by quantitative real time reverse transcription polymerase chain reaction (qRT-PCR). Groups of 15 polyps were amputated sub-hypostomally and placed in a 96-multiwell plate. Untreated and AuNP (1 mg mL^{-1})-treated animals were irradiated with NIR laser at 2.42 W cm^{-2} (Thorlabs, M9-A64-0200) for 1, 5, and 16 h post-amputation. Total RNA was extracted using TRIzol reagent (Thermo Scientific) and its concentration was determined using a SmartSpec plus spectrophotometer (Biorad). The first-strand cDNA was synthesized using High-Capacity cDNA Reverse Transcription Kit (Applied Biosystem) using

0.5 µg of DNA-free RNA in a final volume of 20 µL, according to the manufacturer's instructions. qRT-PCR was performed in 25 µL of the reaction mixture consisting of 1 × Fast SYBR Green Master Mix with premixed ROX (Applied Biosystems), 25 ng of cDNA, and 0.3 mM each primer. The reactions were processed using the StepOne Real-Time PCR System (Applied Biosystem) under the following fast cycling steps: initial denaturation for 20 s at 95 °C, followed by 40 cycles at 95 °C for 3 s, and 60 °C for 30 s. To normalize RNA levels, Hydra EF-1α was used as an internal calibrator. Three technical repeats from three biological replicates were carried out. The delta–delta C_t ($2^{-\Delta\Delta Ct}$) method,[53] for comparing relative expression results between treatments, was applied. Specific primers of *Hydra vulgaris* genes *of EF1α, TCF, Sp5, Myc1, β-cat, FoxO*, and *SOD*, designed using Primer3 software (http://frodo.wi.mit.edu/primer3/) are reported in Table S6 (Supporting Information).

Statistical Analysis: Statistical analysis was performed using GraphPad Prism 9 software.

For gene expression data the One sample t-test or the unpaired t-test were employed. For cell proliferation data the unpaired t-test was employed. Differences in the distribution of regenerative stages were analyzed by Chi-square test. P values: $^{*}P < 0.05$; $^{**}P < 0.01$; $^{***}P < 0.001$.

Supporting Information

Supporting Information is available from the Wiley Online Library or from the author.

Acknowledgements

The authors thank Giuseppe Cacace (CNR-ISASI) for technical assistance in *Hydra* culturing. Figure 5 is created with Biorender.com. Funding: C.T. acknowledges financial support under the National Recovery and Resilience Plan (NRRP), Mission 4, Component 2, Investment 1.1, Call for tender No. 104 published on 2.2.2022 by the Italian Ministry of University and Research (MUR), funded by the European Union – NextGenerationEU, PhageTarget: "Phage platform for targeted antimicrobial photodynamic therapy", CUP B53D23015420006- Grant Assignment Decree No. 1064 adopted on 18/07/2023 by the Italian Ministry of Ministry of University and Research (MUR); C.T. acknowledges financial support under the National Recovery and Resilience Plan (NRRP), Mission 4, Component 2, Investment 1.1, Call for tender No. 1409 published on 14.9.2022 by the Italian Ministry of University and Research (MUR), funded by the European Union – NextGenerationEU– Phoenix: Enhancing tissue regeneration through carbon nanoheaters, CUP B53D23031710001, Grant Assignment Decree No. 1369 adopted on 01/09/2023 by the Italian Ministry of Ministry of University and Research (MUR). N.D.A. acknowledges financial support under the National Recovery and Resilience Plan (NRRP), Mission 4, Component 2, Investment 1.1, Call for tender No. 104 published on 2.2.2022 by the Italian Ministry of University and Research (MUR), funded by the European Union – NextGenerationEU, Rinato: "Unravelling the bases of hyperthermia mediated by gold nanoparticles in a model organism by functional imaging", CUP B53D23020780006- Grant Assignment Decree No. 1065 adopted on 18/07/2023 by the Italian Ministry of Ministry of University and Research (MUR).M.M. acknowledges funding from the European Research Council (ERC) under the European Union's Horizon 2020 research and innovation programme (grant agreement No 853 468).

Conflict of Interest

The authors declare no conflict of interest.

Author Contributions

N.D.A. and M.L.A. contributed equally to this work. Conceptualization was performed by C.T. and A.T. Supervision was performed by C.T and A.T. Methodology was performed by C.T., A.T., M.M, and M.R. Investigation was performed by N.D.A., M.L.A., M.R., and M.M. Original draft was written, reviewed, and edited by C.T.

Data Availability Statement

The data that support the findings of this study are available from the corresponding author upon reasonable request.

Keywords

gold nanoprisms, hydra vulgaris, mild hyperthermia, NIR stimulation, stem cells, tissue regeneration

Received: March 28, 2024
Revised: May 30, 2024
Published online:

[1] a) K. D. Poss, *Nat. Rev. Genet.* **2010**, *11*, 710; b) J. A. Goldman, K. D. Poss, *Nat. Rev. Genet.* **2020**, *21*, 511.
[2] G. C. Gurtner, S. Werner, Y. Barrandon, M. T. Longaker, *Nature* **2008**, *453*, 314.
[3] a) M. E. D. Chaves, A. R. de Araújo, A. C. C. Piancastelli, M. Pinotti, *An Bras Dermatol.* **2014**, *89*, 616; b) N. G. Yeh, C. H. Wu, T. C. Cheng, *Renew Sust Energy Rev.* **2010**, *14*, 2161; c) A. Yadav, A. Gupta, *Photodermatol. Phot.* **2017**, *33*, 4.
[4] A. K. Velichko, E. N. Markova, N. V. Petrova, S. V. Razin, O. L. Kantidze, *Cell. Mol. Life Sci.* **2013**, *70*, 4229.
[5] B. Hildebrandt, P. Wust, O. Ahlers, A. Dieing, G. Sreenivasa, T. Kerner, R. Felix, H. Riess, *Crit. Rev. Oncol. Hemat.* **2002**, *43*, 33.
[6] K. F. Chu, D. E. Dupuy, *Nat. Rev. Cancer* **2014**, *14*, 199.
[7] a) T. Xiang, Q. R. Guo, L. H. Jia, T. Y. Yin, W. Huang, X. Y. Zhang, S. B. Zhou, *Adv. Healthcare Mater.* **2023**, *13*, 2301885; b) G. Cheng, B. Li, *Mater. Today Adv* **2020**, *6*, 10049.
[8] L. F. Li, X. D. Zhang, J. Zhou, L. Q. Zhang, J. J. Xue, W. Tao, *Small* **2022**, *18*, 2107705.
[9] M. Yadid, R. Feiner, T. Dvir, *Nano Lett.* **2019**, *19*, 2198.
[10] a) H. Arami, S. Kananian, L. Khalifehzadeh, C. B. Patel, E. Chang, Y. Tanabe, Y. T. Zeng, S. J. Madsen, M. J. Mandella, A. Natarajan, E. E. Peterson, R. Sinclair, A. S. Y. Poon, S. S. Gambhir, *Nat. Nanotechnol.* **2022**, *17*, 1015; b) A. Gupta, S. Singh, *Small* **2022**, *18*, 2201462.
[11] L. Jauffred, A. Samadi, H. Klingberg, P. M. Bendix, L. B. Oddershede, *Chem. Rev.* **2019**, *119*, 8087.
[12] a) H. Shimizu, Y. Sawada, T. Sugiyama, *Dev. Biol.* **1993**, *155*, 287; b) C. Juliano, J. Cazet, A. Primack, *Innov. Aging* **2022**, *6*, 269; c) T. W. Holstein, E. Hobmayer, U. Technau, *Dev. Dynam.* **2003**, *226*, 257.
[13] a) C. Tortiglione, A. Quarta, M. A. Malvindi, A. Tino, T. Pellegrino, *PLoS One* **2009**, *4*, e7698; b) G. Veronesi, M. Morosll, H. Castillo-Michel, L. Mattera, G. Onorato, K. D. Wegner, W. L. Ling, P. Reiss, C. Tortiglione, *ACS Appl. Mater. Inter.* **2019**, *11*, 35630; c) V. Marchesano, Y. Hernandez, W. Salvenmoser, A. Ambrosone, A. Tino, B. Hobmayer, J. M. de la Fuente, C. Tortiglione, *ACS Nano* **2013**, *7*, 2431.
[14] J. Conde, A. Ambrosone, V. Sanz, Y. Hernandez, V. Marchesano, F. R. Tian, H. Child, C. C. Berry, M. R. Ibarra, P. V. Baptista, C. Tortiglione, J. M. de la Fuente, *ACS Nano* **2012**, *6*, 8316.
[15] A. Ambrosone, P. del Pino, V. Marchesano, W. J. Parak, J. M. de la Fuente, C. Tortiglione, *Nanomedicine* **2014**, *9*, 2829.
[16] M. Moros, A. Lewinska, F. Merola, P. Ferraro, M. Wnuk, A. Tino, C. Tortiglione, *ACS Appl Mater. Inter.* **2020**, *12*, 13718.
[17] M. Moros, A. Ambrosone, G. Stepien, F. Fabozzi, V. Marchesano, A. Castaldi, A. Tino, J. M. de la Fuente, C. Tortiglione, *Nanomedicine* **2015**, *10*, 2167.
[18] B. Pelaz, V. Grazu, A. Ibarra, C. Magen, P. del Pino, J. M. de la Fuente, *Langmuir* **2012**, *28*, 8965.
[19] K. Jiang, D. A. Smith, A. Pinchuk, *J. Phys. Chem. C* **2013**, *117*, 27073.

[20] a) M. Allocca, L. Mattera, A. Bauduin, B. Miedziak, M. Moros, L. De Trizio, A. Tino, P. Reiss, A. Ambrosone, C. Tortiglione, *Environ. Sci. Technol.* **2019**, *53*, 3938; b) A. Ambrosone, L. Mattera, V. Marchesano, A. Quarta, A. S. Susha, A. Tino, A. L. Rogach, C. Tortiglione, *Biomaterials* **2012**, *33*, 1991. c) A. Ambrosone, M. Roopin, B. Pelaz, A. M. Abdelmonem, L. M. Ackermann, L. Mattera, M. Allocca, A. Tino, M. Klapper, W. J. Parak, O. Levy, C. Tortiglione, *Nanotoxicology* **2017**, *11*, 289.
[21] a) L. A. Schroeder, W. M. Callaghan, *Limnol. Oceanogr.* **1981**, *26*, 690; b) T. C. Bosch, S. M. Krylow, H. R. Bode, R. E. Steele, *Proc. Natl. Acad. Sci. USA* **1988**, *85*, 7927.
[22] F. Peebles, *Zoolog. Bullet.* **1898**, *2*, 125.
[23] R. Y. W. Yamamoto, *eNeuro* **2020**, *7*, https://doi.org/10.1523/ENEURO.0539-19.2020.
[24] C. N. Tzouanas, S. Kim, K. N. Badhiwala, B. W. Avants, J. T. Robinson, *iScience* **2021**, *24*, 102490.
[25] a) B. Galliot, M. Miljkovic-Licina, R. de Rosa, S. Chera, *Seminars Cell Developm. Biol.* **2006**, *17*, 492; b) B. Galliot, L. Ghila, *Molecular Reprod. Developm.* **2010**, *77*, 837.
[26] T. C. Bosch, C. N. David, *Dev. Biol.* **1984**, *104*, 161.
[27] a) T. W. Holstein, *Cells Dev.* **2023**, *174*, 203846; b) M. Lechable, M. Achrainer, M. Kruus, W. Salvenmoser, B. Hobmayer, in *Advances in Aquatic Invertebrate Stem Cell Research*, MDPI, Basel, Switzerland **2022**, Vol. *1*; c) S. Siebert, J. A. Farrell, J. F. Cazet, Y. Abeykoon, A. S. Primack, C. E. Schnitzler, C. E. Juliano, *Science* **2019**, *365*, 341.
[28] C. N. David, *Roux Arch Dev. Biol.* **1973**, *171*, 259.
[29] R. D. Campbell, C. N. David, *J. Cell Sci.* **1974**, *16*, 349.
[30] C. N. David, R. D. Campbell, *J. Cell Sci.* **1972**, *11*, 557.
[31] B. M. Mortzfeld, J. Taubenheim, A. V. Klimovich, S. Fraune, P. Rosenstiel, T. C. G. Bosch, *Nat. Commun.* **2019**, *10*, 3257.
[32] A. M. Boehm, K. Khalturin, F. Anton-Erxleben, G. Hemmrich, U. C. Klostermeier, J. A. Lopez-Quintero, H. H. Oberg, M. Puchert, P. Rosenstiel, J. Wittlieb, T. C. Bosch, *Proc. Natl. Acad. Sci. USA* **2012**, *109*, 19697.
[33] D. Bridge, A. G. Theofiles, R. L. Holler, E. Marcinkevicius, R. E. Steele, D. E. Martinez, *PLoS One* **2010**, *5*, e11686.
[34] a) L. Gee, J. Hartig, L. Law, J. Wittlieb, K. Khalturin, T. C. G. Bosch, H. R. Bode, *Dev Biol* **2010**, *340*, 116; b) M. Hartl, S. Glasauer, S. Gufler, A. Raffeiner, K. Puglisi, K. Breuker, K. Bister, B. Hobmayer, *FEBS J.* **2019**, *286*, 2295.
[35] a) M. Hartl, A. M. Mitterstiller, T. Valovka, K. Breuker, B. Hobmayer, K. Bister, *Proc. Natl. Acad Sci. USA* **2010**, *107*, 4051; b) A. Ambrosone, V. Marchesano, A. Tino, B. Hobmayer, C. Tortiglione, *PLoS One* **2012**, *7*, 30660.
[36] a) B. Dash, R. Metz, H. J. Huebner, W. Porter, T. D. Phillips, *Gene* **2007**, *387*, 93; b) V. Malafoglia, F. Del Grosso, M. Scalici, F. Lauro, V. Russo, T. Persichini, D. Salvemini, V. Mollace, M. Fini, W. Raffaeli, C. Muscoli, M. Colasanti, *PLoS One* **2016**, *11*, 0151386.
[37] C. A. Heid, J. Stevens, K. J. Livak, P. M. Williams, *Genome Res.* **1996**, *6*, 986.
[38] a) B. Hobmayer, F. Rentzsch, K. Kuhn, C. M. Happel, C. C. von Laue, P. Snyder, U. Rothbacher, T. W. Holstein, *Nature* **2000**, *407*, 186; b) M. C. Vogg, L. Beccari, L. I. Ollé, C. Rampon, S. Vriz, C. Perruchoud, Y. Wenger, B. Galliot, *Nat. Commun.* **2019**, *10*, 312.
[39] M. Broun, L. Gee, B. Reinhardt, H. R. Bode, *Development* **2005**, *132*, 2907.
[40] G. Onorato, F. Fardella, A. Lewinska, F. Gobbo, G. Tommasini, M. Wnuk, A. Tino, M. Moros, M. R. Antognazza, C. Tortiglione, *Adv. Healthcare Mater.* **2022**, *11*, 2200366.
[41] A. Tursch, N. Bartsch, M. Mercker, J. Schlüter, M. Lommel, A. Marciniak-Czochra, S. Özbek, T. W. Holstein, *Proc. Natl. Acad. Sci. USA* **2022**, *119*, 2204122119.
[42] J. B. Vines, J. H. Yoon, N. E. Ryu, D. J. Lim, H. Park, *Front. Chem.* **2019**, *7*, 167.
[43] a) X. Zhang, G. Cheng, X. Xing, J. Liu, Y. Cheng, T. Ye, Q. Wang, X. Xiao, Z. Li, H. Deng, *J. Phys. Chem. Lett.* **2019**, *10*, 4185; b) Z. Wan, P. Zhang, L. Lv, Y. Zhou, *Theranostics* **2020**, *10*, 11837; c) M. D. M. Encabo-Berzosa, M. Sancho-Albero, A. Crespo, V. Andreu, V. Sebastian, S. Irusta, M. Arruebo, P. Martin-Duque, J. Santamaria, *Nanoscale* **2017**, *9*, 9848.
[44] H. Qin, Y. Chen, Z. Wang, N. Li, Q. Sun, Y. Lin, W. Qiu, Y. Qin, L. Chen, H. Chen, Y. Li, J. Shi, G. Nie, R. Zhao, *Nat. Commun.* **2023**, *14*, 5178.
[45] A. Riedinger, P. Guardia, A. Curcio, M. A. Garcia, R. Cingolani, L. Manna, T. Pellegrino, *Nano Lett.* **2013**, *13*, 2399.
[46] J. T. Dias, M. Moros, P. del Pino, S. Rivera, V. Grazú, J. M. de la Fuente, *Angew. Chem., Int. Ed.* **2013**, *52*, 11526.
[47] A. Alghalayini, L. Jiang, X. Gu, G. H. Yeoh, C. G. Cranfield, V. Timchenko, B. A. Cornell, S. M. Valenzuela, *Biochim. Biophys. Acta Biomembr.* **2020**, *1862*, 183334.
[48] H. Chatterjee, D. S. Rahman, M. Sengupta, S. K. Ghosh, *J. Phys. Chem. C* **2018**, *122*, 13082.
[49] G. Alfranca, A. Artiga, G. Stepien, M. Moros, S. G. Mitchell, J. M. de la Fuente, *Nanomedicine* **2016**, *11*, 2903.
[50] W. F. Loomis, H. M. Lenhoff, *J. Exp. Zool.* **1956**, *132*, 555.
[51] a) O. Wilby, T. M. Tesh, *Toxicol. In Vitro* **1990**, *4*, 582; b) M. Allocca, L. Mattera, A. Bauduin, B. Miedziak, M. Moros, L. De Trizio, A. Tino, P. Reiss, A. Ambrosone, C. Tortiglione, *Environ. Sci. Technol.* **2019**, *53*, 3938.
[52] H. M. Lenhoff, in *Hydra: Research Methods*, (Ed: H. M. Lenhoff), Springer US, Boston, MA **1983**, p. 47.
[53] K. J. Livak, T. D. Schmittgen, *Methods* **2001**, *25*, 402.